



**HAL**  
open science

# Influence of surface integrity on the fatigue behaviour of a hot-forged and shot-peened C70 steel component

B. Gerin, E. Pessard, F. Morel, Catherine Verdu

## ► To cite this version:

B. Gerin, E. Pessard, F. Morel, Catherine Verdu. Influence of surface integrity on the fatigue behaviour of a hot-forged and shot-peened C70 steel component. *Materials Science and Engineering: A*, 2017, 686, pp.121-133. 10.1016/j.msea.2017.01.041 . hal-01804225

**HAL Id: hal-01804225**

**<https://hal.science/hal-01804225>**

Submitted on 5 Dec 2022

**HAL** is a multi-disciplinary open access archive for the deposit and dissemination of scientific research documents, whether they are published or not. The documents may come from teaching and research institutions in France or abroad, or from public or private research centers.

L'archive ouverte pluridisciplinaire **HAL**, est destinée au dépôt et à la diffusion de documents scientifiques de niveau recherche, publiés ou non, émanant des établissements d'enseignement et de recherche français ou étrangers, des laboratoires publics ou privés.

# Influence of surface integrity on the fatigue behaviour of a hot-forged and shot-peened C70 steel component

Benjamin Gerin<sup>a,b,\*</sup>, Etienne Pessard<sup>a</sup>, Franck Morel<sup>a</sup>, Catherine Verdu<sup>b</sup>

<sup>a</sup> LAMPA, Arts et Métiers ParisTech Angers, 2 Bd du Ronceray, 49035 Angers Cedex 01, France

<sup>b</sup> MATEIS, INSA de Lyon, Bâtiment St Exupery, 20 av Jean Capelle, 69621 Villeurbanne Cedex, France

## Keywords:

Steel  
Forging  
Shot-peening  
High cycle fatigue  
Surface defects  
Residual stresses

## A B S T R A C T

Hot-forging is a process commonly used in the manufacturing of automobile parts such as connecting rods. Most hot-forged components are shot-blasted after forging in order to clean off the forging scale. The shot-blasting process is akin to shot-peening and greatly affects the surface integrity of the components by introducing hardening and residual stresses. This study focuses on the influence of the surface integrity on the fatigue behaviour of a hot-forged C70 steel connecting rod. Specimens were machined out of the connecting rods in order to perform fatigue testing on the forged surface. Several surface states, including shot-peened surfaces, were studied in order to quantify the influence of the surface integrity.

A thorough characterisation of the surface integrity of the specimens was first performed. The hardness, residual stresses and microstructure gradients were analysed, and the surface of each specimen was scanned using a profilometer. The specimens show complex networks of surface defects introduced during forging, and the shot-blasting process introduces important surface residual stress and microstructure gradients. High cycle fatigue tests in plane bending were then performed on the specimens, with the surface scans helping to identify the critical defect on which crack initiation occurred. The fatigue results, presented in the form of a Kitagawa diagram, are analysed in order to determine which surface integrity parameters are the most influential on fatigue behaviour. The forging defects have an important negative effect on fatigue strength. After shot-blasting, the fatigue strength increases considerably because of the large compressive residual stresses introduced by the shot-blasting process.

## 1. Introduction

Hot-forging is a process commonly used in the manufacturing of automobile parts. The expensive dies used for this process mean it is mainly used for mass production. Connecting rods for an internal combustion engine are a typical example of components manufactured with this process.

Hot-forging requires heating the material to high temperatures in order to achieve sufficient ductility (typically 1000 °C for steel). The subsequent phase transition during cooling means that the resulting microstructure shows little to none of the hardening or the residual stresses introduced during forming.

However, the high temperature increases oxidation and often a layer of oxides, called forging scale, is formed on the surface of the components. This layer must be removed before the next steps of the manufacturing process can be performed (sizing, machining, etc).

A very common method for cleaning off the scale is the shot-blasting process [1]. Several hundred components are placed in a

rotating barrel while steel shot is propelled into the barrel (Fig. 1a). Shot-blasting is therefore similar to shot-peening but does not have the same purpose, as shot-peening is used to introduce compressive residual stresses and also to change surface roughness (Fig. 1b). Both processes (shot-blasting and shot-peening) introduce local plastic strain with each shot impact, resulting in hardening and internal stresses near the surface of the components.

During forging, defects can appear on the surface of the components. Between two strikes, scale can get stuck on the dies' surface, generating surface defects the size of which can reach several millimeters in length and several hundred micrometers in depth. Shot-blasting does not remove the largest of these forging defects. Surface defects are potentially very harmful in fatigue, which is why it is important to study their impact on fatigue behaviour [2].

The oxidation during forging can also lead to decarburisation of the surface: the carbon content decreases which directly impacts the mechanical characteristics, most notably hardness. Gildersleeve [3] studied the influence of surface carbon content on the fatigue strength

\* Corresponding author at: LAMPA, Arts et Métiers ParisTech Angers, 2 Bd du Ronceray, 49035 Angers Cedex 01, France.  
E-mail address: benjamin.gerin@ensam.eu (B. Gerin).

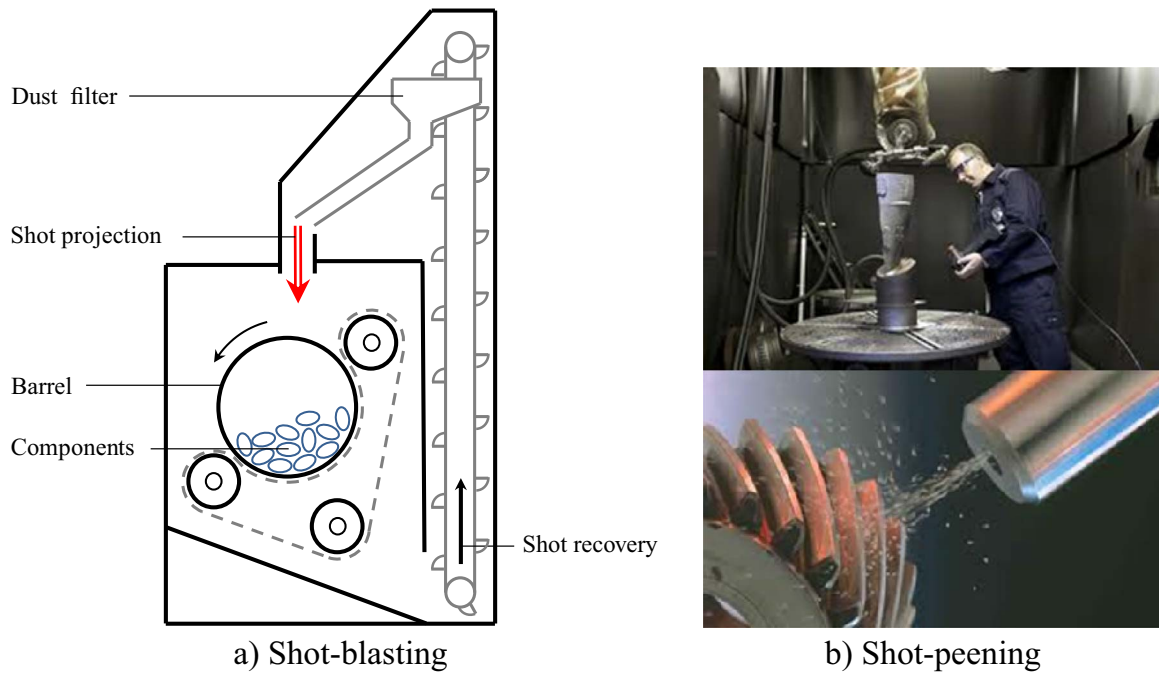


Fig. 1. a) Diagram of the shot-blasting process. b) Photos illustrating the shot-peening process, source: Metal Improvement Company.

of steel specimens. Using controlled decarburisation to modify the carbon content, he found that fatigue strength was proportional to surface hardness and followed the empirical law suggested by Garwood et al. [4]:  $\sigma^D = 1.5 \times H_v$ .

McKelvey & Fatemi [5] performed fatigue tests on hot-forged specimens, studying the effects on fatigue of decarburisation and shot-cleaning of the surface. They showed that the as-forged surface has a much lower fatigue strength compared to polished specimens (50% to 70% drop) because of the combined effects of surface roughness and decarburisation. The severity of the decarburisation depends on the heating process, with induction heating leading to less decarburisation than gas heating. They also showed that the use of shot-cleaning on the as-forged surface improves fatigue strength, independently of decarburisation.

Numerous studies have been conducted on how shot-peening affects surface integrity. Gariépy et al. [6] conducted a thorough characterisation of the surface of a shot-peened aluminium, measuring the hardness, microstructure and residual stresses gradients generated near the surface. They also showed that shot-peening increases roughness and creates surface micro-defects.

The influence of shot-peening on fatigue behaviour has also been extensively studied. Bhuiyan et al. [7] investigated shot-peened magnesium alloy specimens, some of which were stress-relieved after peening. They showed that the fatigue strength depends on the combined effects of the compressive residual stresses (which improve the fatigue strength), and the roughness (which decreases fatigue strength).

Sakamoto et al. [8,9] performed fatigue tests on steel specimens, polished or shot-peened. Focused ion beam (FIB) was used to introduce small surface notches (50  $\mu\text{m}$ ) in some of the specimens. The fatigue results showed that the notches reduced the fatigue limit for the polished specimens, but not the shot-peened ones. The shot-peened specimens had multiple crack initiations, on the notches and on cracks generated by the shot-peening. These results show that surface defects have no effect on the fatigue behaviour of a shot-peened surface if they have the same size as the cracks generated by the shot-peening.

Fathallah et al. [10] studied the effect on fatigue behaviour of shot-peening coverage. They performed characterisations and fatigue tests

on steel specimens with 100% or 1000% surface coverage. They found that 1000% coverage had bigger surface defects and lower surface residual stresses than 100% coverage. To model the fatigue behaviour, they performed 2D finite element simulations, taking into account the specimen geometry, the surface defects, the surface damage, the residual stresses and the hardening introduced by shot-peening. Their model correctly predicted the experimental fatigue limits and showed that ignoring the effects of the defects and the surface damage would lead to predicting crack initiation not on the surface but at the depth where the residual stresses reach zero.

These articles show that the surface integrity of forged components is the combination of different aspects that can all have an effect on fatigue behaviour. These aspects result from the hot-forging or the subsequent shot-blasting.

From forging:

- Large surface defects
- Decarburisation

From shot-blasting:

- Surface roughness
- Hardening gradient
- Residual stresses
- Microstructure gradient
- Surface micro-defects

These aspects all influence fatigue behaviour differently, and are not easily studied independently, especially in the case of shot-blasting where all are introduced simultaneously. Very few articles have managed to decouple the various effects of the surface integrity.

The goal of the present study is therefore to analyse the fatigue strength and the crack initiation mechanisms for specifically chosen surface integrity conditions. First, the various aspects of the surface integrity will be thoroughly characterised, then fatigue tests will be conducted in order to quantify their effect on fatigue behaviour. The fatigue results will serve to decouple the various surface integrity factors affecting fatigue behaviour.

**Table 1**  
Chemical composition C70 steel, in weight percentage.

Element	C	Si	Mn	S	P	Ni	Cr	Mo
Min	0.690	0.150	0.530	0.0600			0.100	
Value	0.707	0.170	0.569	0.0660	0.015	0.051	0.177	0.024
Max	0.730	0.250	0.600	0.0700	0.030	0.180	0.200	0.050
Element	Cu	Al	Sn	V	Te	Se	N <sub>2</sub>	
Min				0.030			0.01200	
Value	0.086	0.000	0.008	0.034	0.0030	0.0000	0.01420	
Max	0.250	0.010	0.025	0.040	0.0030	0.0050	0.00170	

## 2. Experimental procedure for studying various surface integrities

The component chosen for this study is a hot-forged connecting rod produced by Atelier des Janves (ADJ) and used in certain Renault engines. The connecting rods are produced from round bars of C70 steel. These bars are hot-rolled and air-cooled resulting in a pearlitic microstructure.

### 2.1. Mechanical properties of the C70 steel

The chemical composition of the C70 steel are given in Table 1 and its mechanical properties after forging are given in Table 2. Hardness was measured along the cross-section using a microdurometer.

### 2.2. Studied industrial component: hot-forged connecting rod

The steps for the production of the connecting rods are:

- Cutting the steel bar
- Induction heating of the workpiece
- Cross rolling to obtain the preform
- Stamping of the connecting rod in three passes
- Deburring (while hot)
- Sizing (while hot)
- Controlled air-cooling on a belt conveyor
- Shot-blasting
- Quality control

After forging, the connecting rods also have a pearlitic microstructure.

The study is restricted to the flat central part of the connecting rod, with fatigue specimens machined out of the connecting rod beam using spark machining (Fig. 2a). Restricting the study to a flat area makes analysing the surface much easier and avoids local stress concentrations due to specimen geometry. Fig. 2b shows the geometry of the specimens.

The specimens were machined so as to leave the surface of the middle section unaltered. The corners of the specimens were rounded and the machined sides were polished to prevent crack initiation outside of the studied surface.

### 2.3. Studied batches

In order to quantify the influence of the various aspects, it is necessary to study different surface states and to compare them. ADJ

**Table 2**  
Mechanical characteristics of the C70 steel (measured on as-forged specimens).

	$\sigma_{YS}$ MPa	$\sigma_{UTS}$ MPa	$A_r$ %	Hardness H <sub>v</sub> 0.1 kg Average $\pm$ Std. deviation
C70 steel	598	1020	15.6	292 $\pm$ 11

delivered 688 shot-blasted connecting rods and 485 as-forged (without shot-blasting), taken from their production line. The forging scale was still present on the as-forged connecting rods so those used in the study were manually cleaned with a metal brush in order to avoid damaging the surface or introducing residual stresses. It was decided to use shot-peening to obtain specific surface states, different from that of shot-blasting. Shot-peening is similar to shot-blasting but with a high degree of control on the peening parameters meaning that it is possible to obtain specific surface states. Two shot-peening batches were chosen: the first replicates the shot-blasting surface state and the second has a lower roughness and a shallower residual stress profile. The shot-peening was performed by the Metal Improvement Company on specimens machined out of as-forged connecting rods (manually cleaned of scale). In order to have a reference for the fatigue tests, some specimens were ground and mirror-polished so as to have a surface state with no hardening, no defects.

The various surface states used in this study are as follows:

- As-forged surface, manually cleaned of scale
- Shot-blasted, the surface state of industrially produced connecting rods
- Shot-peened with shot diameter 800  $\mu$ m, Almen intensity 3060 A with 200% coverage. This shot-peening was performed on as-forged specimens and was chosen so as to be as close as possible to the shot-blasted surface.
- Shot-peening with shot diameter 400  $\mu$ m, Almen intensity 2030 A with 200% coverage. This shot-peening was performed on as-forged specimens and was chosen so as to have a lower roughness and a shallower residual stress profile.
- Polished, used as the reference in fatigue

Fig. 3 shows specimens from each batch and details how the specimens were prepared.

## 3. Surface defects, residual stresses and microstructural characteristics for the different surface integrities

The various batches have different surface states but have all the same core properties, determined with tensile tests and microhardness measurements. The surface state of each batch was analysed as follows:

- Microhardness measurements
- X-ray diffraction analysis of the residual stresses
- Surface topography measurements with a profilometer
- Scanning electron microscope (SEM) and electron backscatter diffraction (EBSD) imaging of the microstructure

### 3.1. Microstructure and residual stresses

The as-forged specimens have a pearlitic microstructure, which shows no gradient from the core to the surface. Furthermore, the microstructure is the same for the long and transverse directions. The microstructure of the specimens is therefore homogeneous and isotropic, which is generally the case in hot-forging. SEM images and EBSD maps of the polished cross-section of as-forged specimens are shown in Fig. 4. EBSD gives a visual representation of the ferrite grain orientations, showing the impact of the extrusion on the grains. Characterisation was performed on a Zeiss Supra VP55 SEM with a field-emission gun, operated at 15 kV and equipped with an Oxford-Instruments EBSD camera. A step size between 0.4 and 0.1  $\mu$ m was used depending on magnification. It should be noted that the cementite is not visible in the EBSD maps, meaning that only the ferrite grains are mapped.

The SEM images show the surface microstructure of these specimens remains pearlitic, even just beneath residual scale. These observations indicate that no decarburisation occurred during the

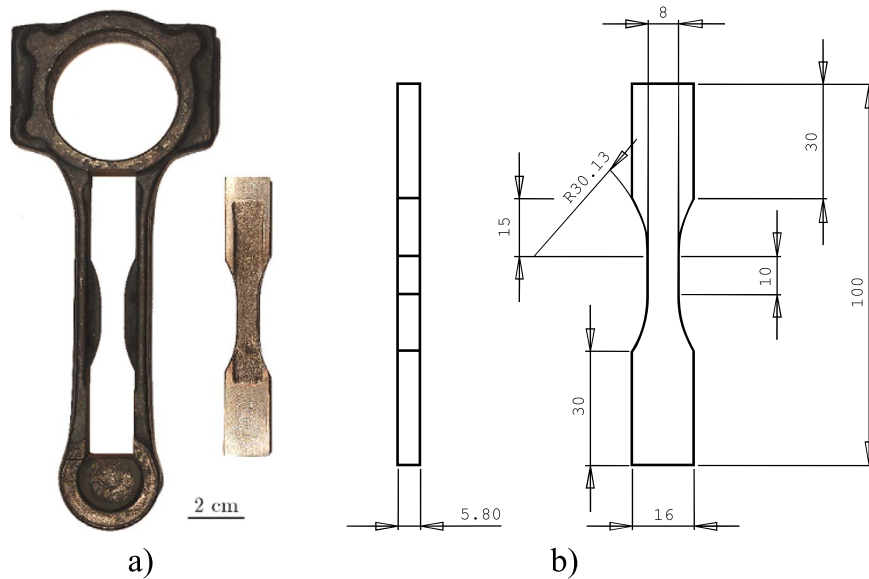


Fig. 2. a) Connecting rod with spark-machined specimen. b) Engineering drawing of the specimens machined out of the connecting rods.

forging process. This is due to ADJ controlling the forging and cooling parameters in order to reduce decarburisation as much as possible.

After shot-blasting and shot-peening, the specimens show a clear microstructure gradient near the surface of shot-blasted specimens (Fig. 5). This surface microstructure can be divided into four layers:

1. A surface layer 5–10  $\mu\text{m}$  deep where the grains are extremely small
2. A second layer around 20  $\mu\text{m}$  deep with heavily deformed grains
3. A transition layer 100–150  $\mu\text{m}$  deep where the grains are progressively less deformed
4. The unaffected core material (not shown in Fig. 5)

These layers are the same as those observed by Gariépy et al. [6] on a shot-peened aluminium alloy.

Fig. 6 shows SEM and EBSD images of a surface fold generated during shot-blasting, with trapped scale. The scale was not detected during EBSD mapping and appears white in the image. Additionally, cracks running parallel to the surface were detected in the shot-blasted surface, likely resulting from grain delamination during impact. Feng et al. [11] have observed similar microdefects in ultrasonic peening and have shown that they can have a negative impact on fatigue behaviour.

Fig. 7 shows examples of the shot-blasted surface integrity which all have a potential effect on fatigue behaviour.

Fig. 8 shows the surface hardness gradient up to a depth of 1 mm for all batches. For the as-forged batch, the surface hardness is close to

the core value which confirms the absence of decarburisation. The shot-blasted and shot-peened batches show a clear increase in hardness near the surface, with a surface value around 50  $H_V$  higher than the core value.

The residual stresses were analysed using X-ray diffraction. A PROTO iXRD machine was used, equipped with a Cr anode vacuum tube and two PSD detectors. The  $K\alpha$  radiation of the Cr target has a wavelength of  $\lambda = 0.22909 \text{ nm}$ . The diffracting planes are the  $\{211\}$  planes of the BCC structure of the ferrite, with a Bragg angle of  $2\theta = 156.4$ . The crystallographic elastic constants used were:  $S_1 = -1.28 \times 10^{-6} \text{ MPa}^{-1}$  and  $\frac{1}{2}S_2 = 5.92 \times 10^{-6} \text{ MPa}^{-1}$ . The first measure (zero depth) is made on the specimen surface, with deeper measurements obtained by locally removing thin surface layers through electropolishing. Fig. 9 shows the residual stress profiles of all batches. The as-forged surface shows negligible residual stresses, which is expected in hot-forging. Shot-blasting produces a residual stress profile which does not have the standard bell-shape seen in shot-peening. Instead, the highest value is located on the surface ( $-500 \text{ MPa}$ ) and the profile gradually decreases to reach a value close to zero at a depth of around 500  $\mu\text{m}$ . Both shot-peened surfaces have the expected profiles: shot-peening with  $\varnothing 800 \mu\text{m}$  shot has a profile very close to that of the shot-blasting, and shot-peening with  $\varnothing 400 \mu\text{m}$  shot has the same surface value but half the depth. Shot-blasting and shot-peening do not favour specific orientations, so the stress values are similar in both directions.

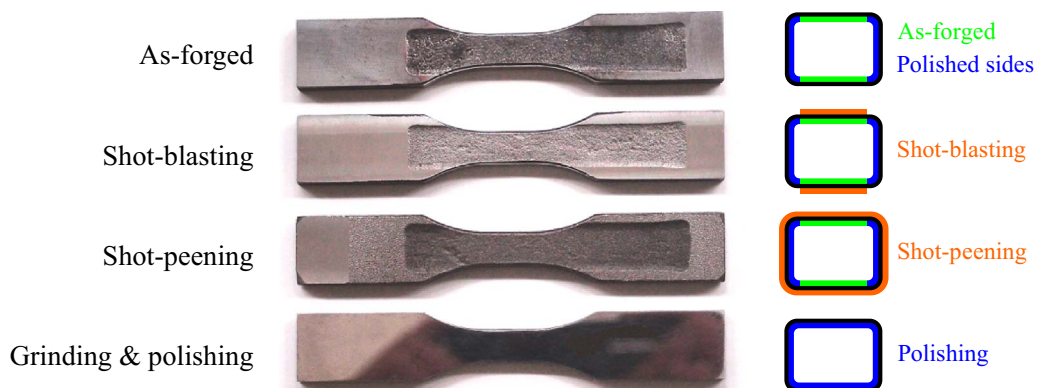


Fig. 3. Specimens from each batch with cross-section detailing the specimen preparation.

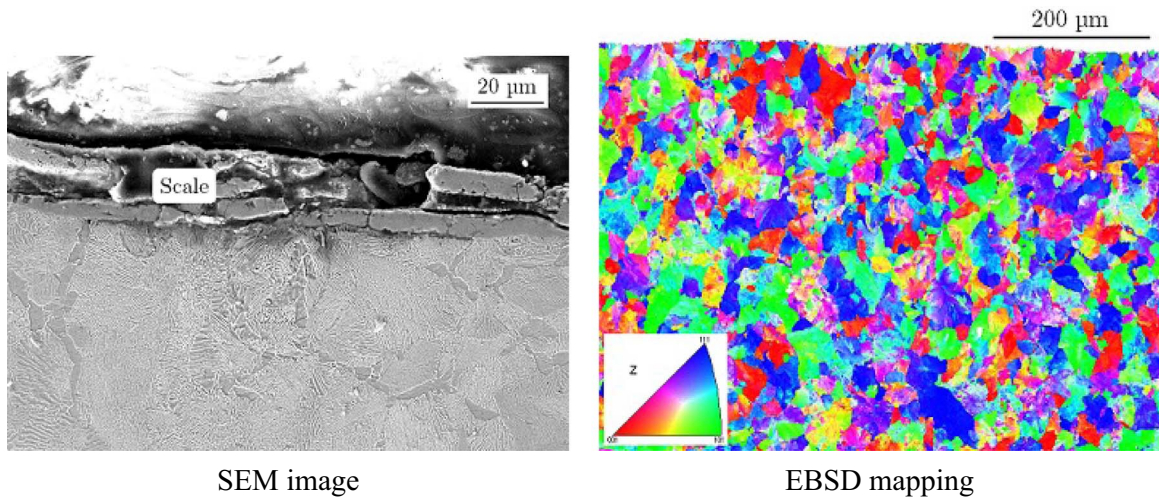


Fig. 4. SEM image and EBSD mapping of the surface microstructure for the as-forged batch.

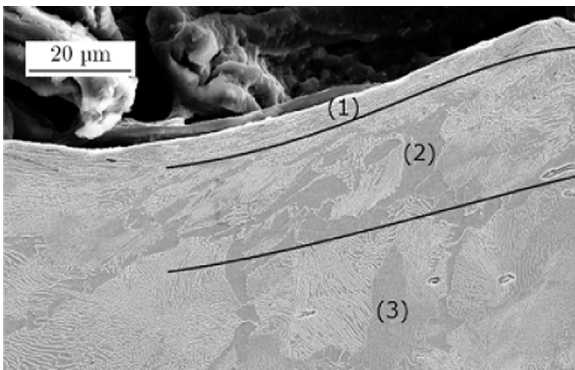


Fig. 5. Microstructure gradient of a shot-blasted specimen.

### 3.2. Roughness and surface defects

3D surface scans of the specimens were made using a Bruker ContourGT-K0-X profilometer. All specimens were scanned before and after fatigue testing, in order to easily analyse the crack initiation location. Fig. 10 shows a 2×2 mm close-up for each batch. Each batch has an unique topography which makes it easily distinguishable from the others. The forging defects are clearly visible on the as-forged surface, and the defects are not completely erased after shot-blasting or shot-peening. Individual shot impacts are visible on both shot-peened surfaces, and the difference in shot diameter can be seen clearly. In the

case of the shot-blasted surface, the individual impacts are not easily visible. This is because for shot-blasting, the shot is not often replaced, instead the same batch is re-used repeatedly. This means that while the shot diameter is initially 1 mm, wear and fragmentation during shot-blasting lead to very varied shot sizes.

The surface scans were also used to measure roughness values for each batch. The results are given in Table 3. The roughness values are very similar for the as-forged and the shot-peened Ø400 µm shot surfaces, despite the fact that the two surfaces are easily distinguished visually. The same is also true for the shot-blasted and the shot-peened Ø800 µm shot surfaces. This means that the roughness values do not accurately reflect the differences in surface topography between the various batches. This is due to the forging defects which have a high roughness value even before shot-peening.

## 4. Fatigue strength and crack initiation mechanism

### 4.1. Plane bending fatigue tests

The fatigue tests were performed in plane bending with a load ratio of  $R = -1$ . This load ratio was chosen as it creates the highest loading stress on the specimen surface and therefore favours crack initiation in the studied surface and not the machined sides of the specimens. Fatigue tests were performed on a RUMUL Cracktronic resonant fatigue testing machine, at a frequency of 80 Hz. The surface of each specimen was scanned before fatigue testing and after crack propaga-

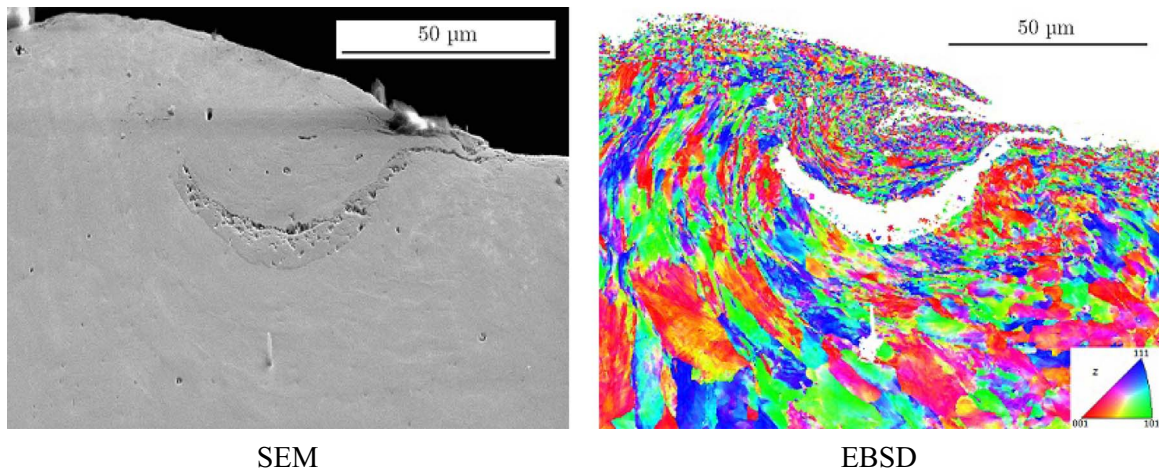
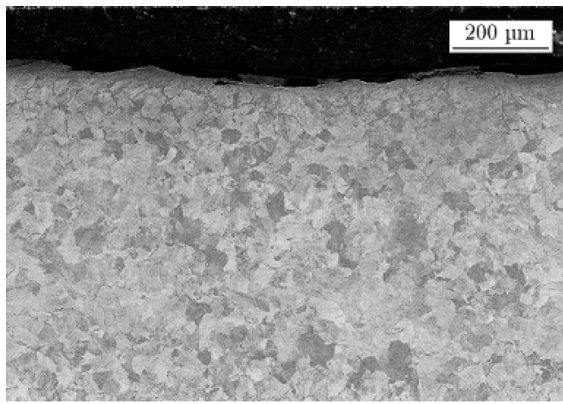
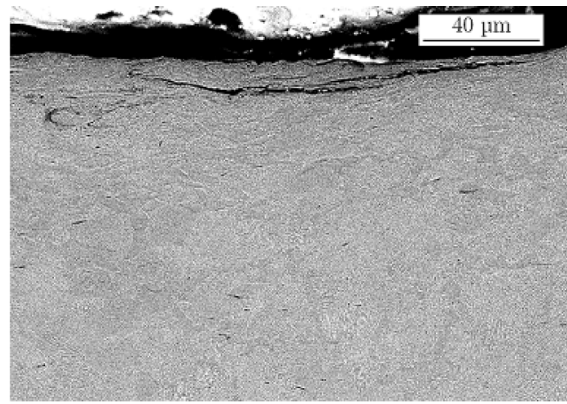


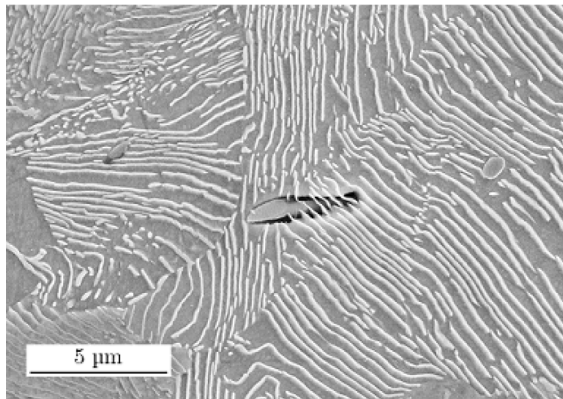
Fig. 6. SEM and EBSD images of the same fold in a shot-blasted specimen. The trapped scale was not detected during EBSD mapping.



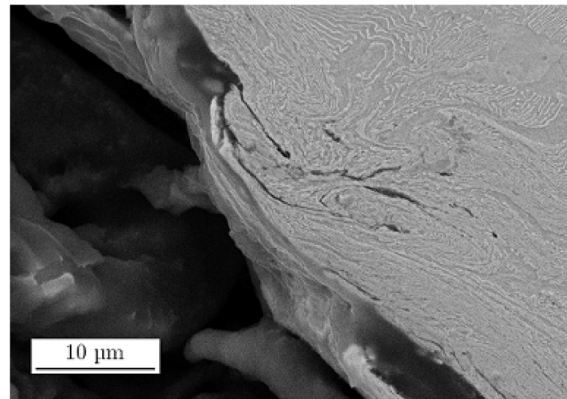
Roughness (shot impacts)



Cracks



Inclusions



Damage

Fig. 7. SEM images showing the various aspects of the surface integrity of shot-blasted specimens.

tion. This, combined with SEM observation of the fracture surface, allowed to confirm that crack initiation had occurred on the studied surface and to locate the crack initiation on the undamaged surface scan.

A staircase method was performed on 15 specimens for the polished batch. The staircase method [12] determines the fatigue limit using multiple specimens. The first specimen is cycled with a load close to the expected fatigue limit. If a specimen survives the  $2 \cdot 10^6$  cycles, the loading value is increased for the next specimen. If a specimen fails, loading is decreased for the next specimen. Loading is increased or decreased by a fixed value chosen so as to be small enough to accurately reflect the fatigue dispersion without leading to too many load levels (generally 10–25 MPa). After all specimens have been cycled, a

statistical analysis determines the fatigue limit.

For the batches other than the polished specimens, the "Locati" step method was used in order to determine a fatigue strength value for each specimen. This method was previously used for a similar study performed on cold-forged components [13] and also by other authors [14].

#### 4.2. Residual stress analysis during fatigue testing

The residual stresses potentially have a large impact on fatigue behaviour, which is why it is important to know if stress-relief occurs during fatigue cycling. Kang et al. [15] have shown that for high-cycle fatigue, the surface residual stresses have only minimal stress-relief. In

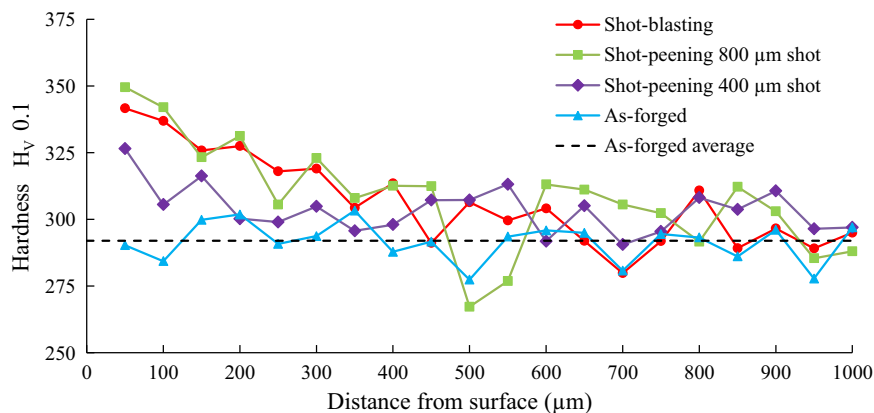


Fig. 8. Surface hardness gradients for the various batches.

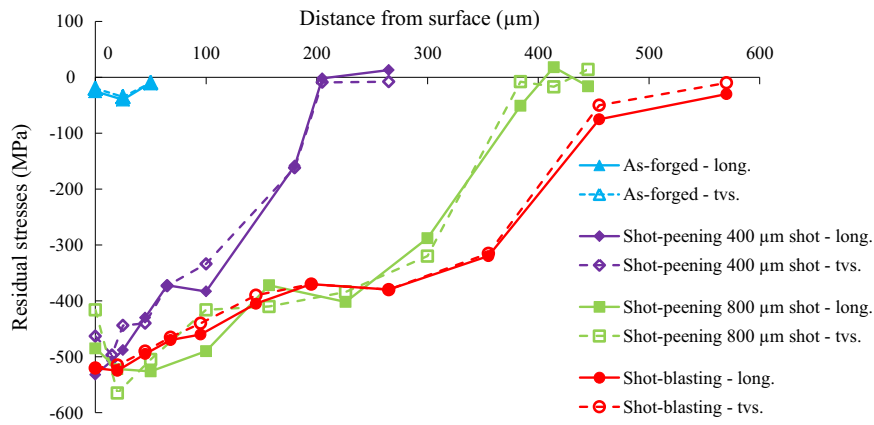


Fig. 9. Residual stress profiles for the various batches, in the direction of the specimen axis (long.), and the transverse direction (tvs.).

order to quantify stress-relief, a shot-blasted specimen with a large surface defect was chosen; surface residual stresses were analysed in the centre of the specimen and in the defect. The specimen was then loaded in fatigue at a high stress value of 475 MPa, and the test was periodically stopped to perform new measurements of the residual stresses. Fig. 11 shows the location of the residual stress analysis on the

surface scan of the specimen, and the results of the measurements with the corresponding number of cycles. The specimen failed at 139, 400 cycles, with the crack initiation located at the defect. For the first 100,000 cycles, the surface residual stresses show almost no change in value, both at the centre of the specimen and in the defect. These results show that no stress relief occurs during fatigue cycling, the

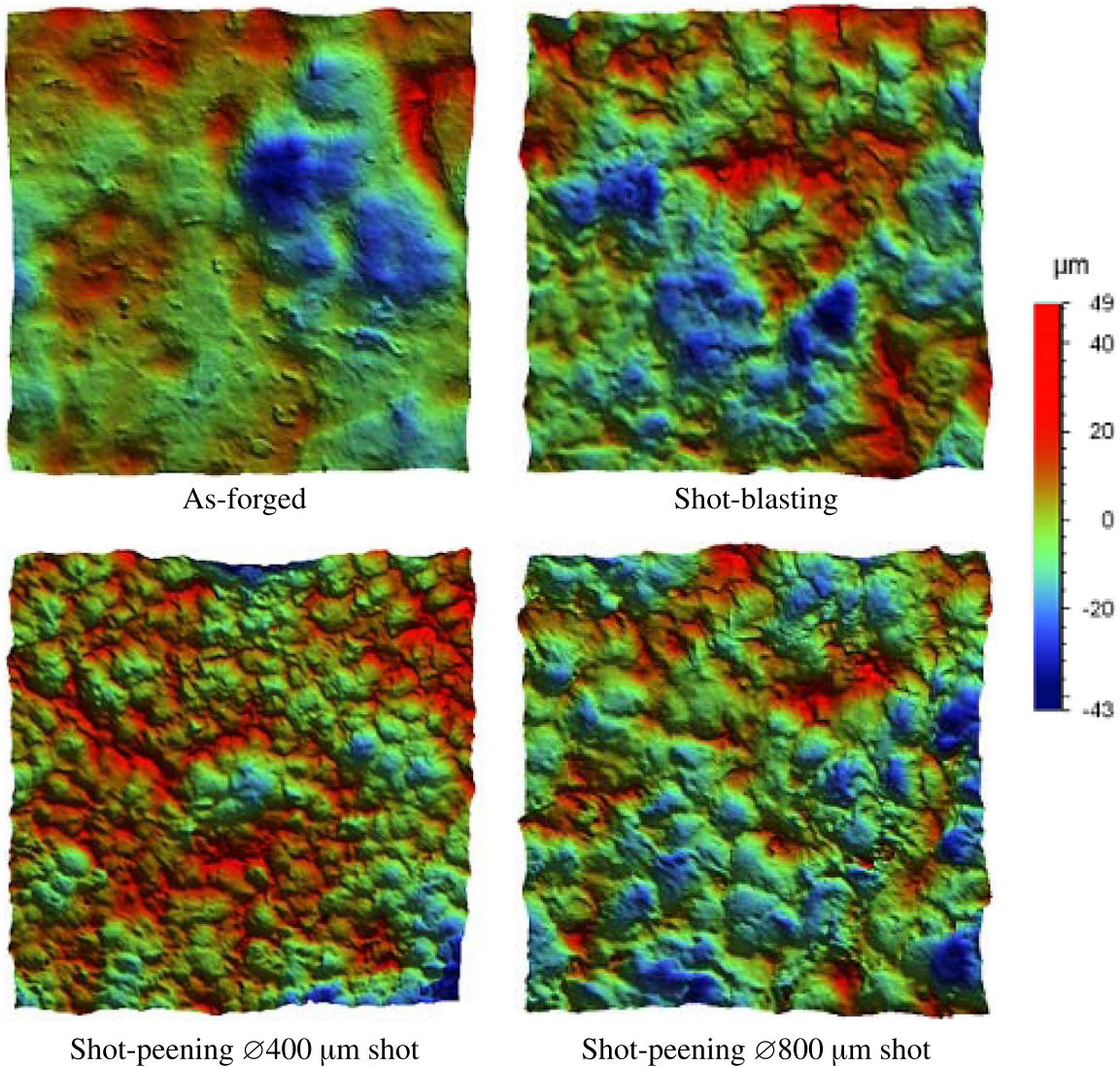


Fig. 10. Close-ups of surface scans of the specimens, for each batch. Surfaces have a size of 2×2 mm with Z scale in μm.

**Table 3**

Roughness values for each batch. Measuring length: 12.5 mm; cut-off length: 2500  $\mu\text{m}$ .

Surface state	$R_a$ and std. deviation ( $\mu\text{m}$ )	$R_z$ ( $\mu\text{m}$ )	$S_a$ ( $\mu\text{m}$ )	$S_z$ ( $\mu\text{m}$ )
As-forged	6.44 $\pm$ 2.01	46.11	10.08	122.33
Shot-blasting	7.83 $\pm$ 0.92	58.77	10.66	160.40
Shot-peening $\varnothing$ 800 $\mu\text{m}$ shot	7.64 $\pm$ 0.81	64.86	11.62	153.28
Shot-peening $\varnothing$ 400 $\mu\text{m}$ shot	6.34 $\pm$ 1.64	49.44	11.41	138.61

residual stresses are therefore assumed to keep their initial value during fatigue testing.

### 4.3. Fatigue testing results

In addition to bending fatigue tests, some tension fatigue tests were also performed, using a hydraulic testing machine.

In order to quantify the effect of the residual stresses on fatigue behaviour, some specimens were stress-relieved by applying a 1% elastic deformation in tension. Residual stress analysis before and after deformation were made to confirm that the deformation had relieved most of the residual stresses in the longitudinal direction. The residual stresses in the transverse direction were unaffected.

Not all specimens resulted in successful fatigue tests, as some crack initiations occurred in the specimen corners or on the machined sides. All the specimens which did not have a crack initiation located on the studied surface were discarded.

Only one of the tension tests was valid, performed on a stress-relieved shot-peened  $\varnothing$ 800  $\mu\text{m}$  shot. This test was the only valid stress-relieved test, as all the others had a corner crack initiation.

Table 4 details the number of valid specimens for each batch, with their respective fatigue strength range. The average value from the staircase method on the polished specimens is the reference fatigue strength of the material:  $\sigma_0^D = 424$  MPa.

Additional tests were performed on specimens which were ground prior to shot-peening, in order to remove the forging defects. Some of these specimens were also stress-relieved. Because of the absence of the forging defects, the crack initiation for these defects was always occurred in the specimen corners (special care was taken to the peening of the corners during shot-peening). A staircase of five specimens was performed on ground and shot-peened  $\varnothing$ 400  $\mu\text{m}$  shot specimens, giving a fatigue strength of 488 MPa. Another staircase was performed on five stress-relieved specimens (ground and shot-peened  $\varnothing$ 400  $\mu\text{m}$ ), resulting in a fatigue strength of 388 MPa. The fatigue results for these staircases specimens cannot be directly exploited, however, comparing the results of these two batches shows a 100 MPa drop in fatigue strength after stress-relief.

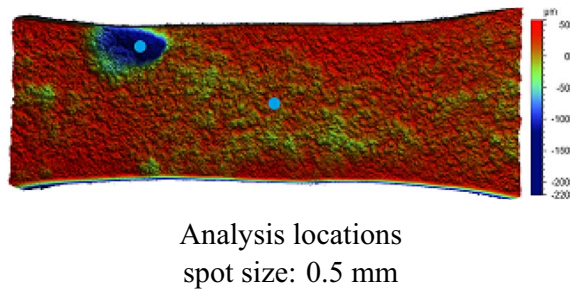


**Fig. 11.** Surface residual stresses analysis performed during the fatigue test of a shot-blasted specimen. The location of the measurements are indicated on the surface scan of the specimen.

**Table 4**

Overview of the number of valid tests and fatigue strength range for each batch.

Batch	Test type	Nbr. of specimens	$\sigma^D$ (MPa)
Polished	Staircase	15	424
As-forged	Locati	34	280–400
Shot-blasting	Locati	8	420–500
Shot-peening $\varnothing$ 800 $\mu\text{m}$ shot	Locati	10	500–580
Shot-peening $\varnothing$ 400 $\mu\text{m}$ shot	Locati	18	400–500
<b>Tension SP <math>\varnothing</math>800 <math>\mu\text{m}</math> shot stress-relieved</b>	Locati	1	431

### 4.4. Crack initiation mechanism

For all the valid specimens (except the polished batch), crack initiation was located on a large forging defect. This defect is called the critical defect because it is the defect which led to crack initiation first. Fig. 12 shows examples of the fracture surface with the critical defect for specimens of each batch. Crack initiation was always located on the surface, for all batches (Fig. 13). For the shot-blasted and shot-peened specimens, the crack initiation is therefore influenced by both the large forging defects and the microdefects introduced by the shot-blasting and shot-peening processes.

Each specimen having been scanned prior to fatigue testing, the critical defect can be identified on the surface scans using the fracture surface analysis. Fig. 14 shows the surface scan and a close-up of the critical defect of the as-forged specimen shown in Fig. 12.

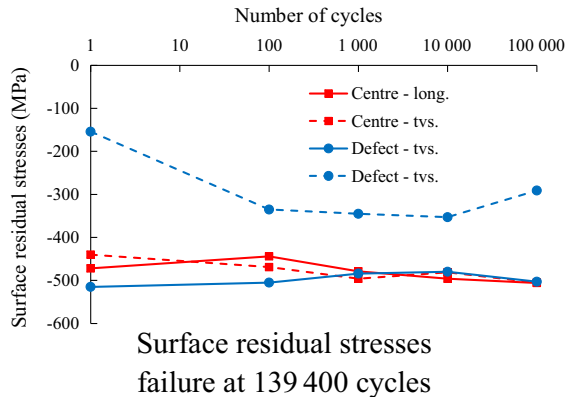
## 5. Analysis and discussion

### 5.1. Fatigue trend for each batch

Defect size is represented using the square root of their surface area, projected along the loading direction [16]. The fracture surfaces can be used to calculate the projected surface area of each critical defect, which is generally used to represent defect size. All the defects have a projected area of similar shape, with the width much bigger than the depth (defects are typically 500–2000  $\mu\text{m}$  wide and 50–200  $\mu\text{m}$  deep). Calculating the projected area is done using the SEM fracture surface images: the total width and maximum depth of the defects are measured and their projected surface area is calculated by supposing that they have a semi-elliptical shape:

$$\text{area} = \frac{\pi a c}{2} \quad (1)$$

with  $a$  being half the defect's width (total width is  $2a$ ) and  $c$  its depth. As suggested by Murakami, the defect width is limited by a threshold of 10 times the depth when calculating the projected area.



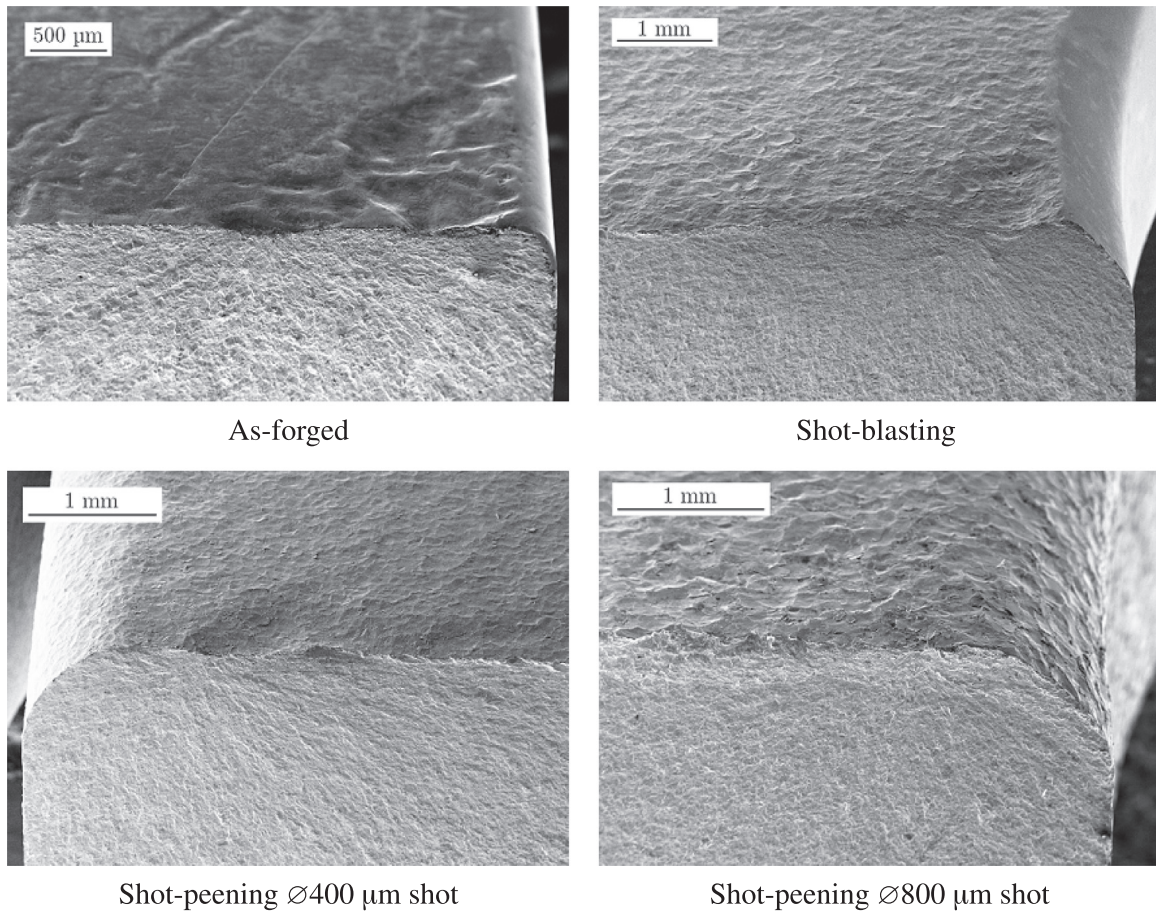


Fig. 12. SEM images of fracture surfaces showing the critical defect at the origin of crack initiation for each batch.

The fatigue results are represented in a Kitagawa diagram [17] (Fig. 15).

- **As-forged specimens:** the fatigue strength is always lower than the reference fatigue strength  $\sigma_0^D = 424$  MPa. This is due solely to the forging defects, as these specimens have no hardening or residual stresses. This batch has a high dispersion in fatigue strength, however a bigger defects tend to have a greater impact on fatigue strength. The lowest fatigue strength is 140 MPa lower than the reference fatigue strength, which is a 34% drop.
- **Shot-blasted and shot-peened specimens:** the fatigue strength is generally much higher than the reference, which means that shot-blasting and shot-peening have a very positive effect on fatigue behaviour. The highest fatigue strength is 150 MPa higher than the reference (35% increase). However, this does not negate the influence of the forging defects: the biggest defects also have the lowest fatigue strengths. At equivalent defect sizes, shot-blasted and shot-peened specimens have a fatigue strength around 150 MPa higher than the as-forged specimens, which is an increase of roughly 50%. The shot-blasted specimens all have large defects because all the other specimens in the batch had corner crack initiations and were thus discarded. For equivalent defect sizes, the shot-blasted and shot-peened  $\varnothing 400$   $\mu\text{m}$  shot specimens have the same fatigue strength. The two shot-peened batches do not have quite the same fatigue strength, with the  $\varnothing 400$   $\mu\text{m}$  shot being around 50 MPa lower.

Some shot-peened specimens were scanned before and after shot-peening in order to analyse the influence of shot-peening on defects. Two (non critical) defects of similar size and shape were chosen. Fig. 16 shows the surface scans before and after shot-

peening.

The after shot-peening surfaces have been altered but the general shape of the defects remains unchanged. However, it seems that the shot-peening  $\varnothing 800$   $\mu\text{m}$  shot has a greater impact on defect geometry.

- **Stress-relieved specimen:** only one stress-relieved specimen was valid, of the shot-peening  $\varnothing 800$   $\mu\text{m}$  shot batch, loaded in tension. The fatigue strength for this specimen is 431 MPa, which is, for the same defect size, roughly 70 MPa lower than the non-stress-relieved specimens (800  $\mu\text{m}$  batch) and 100 MPa higher than the as-forged specimens. This drop of the fatigue strength after stress-relief has been confirmed with the ground and shot-peened specimens, which show a consistent drop of around 100 MPa after stress-relief. These results show that the residual stresses have a very beneficial influence on fatigue behaviour. However, relieving the residual stresses in the loading direction was not enough to lower the fatigue strength to the level of as-forged specimens. This could be due to the hardening generated by the shot-peening which was not affected during stress-relief. However, it is also possible that the residual stresses in the transverse direction, which remained unchanged, could also have an influence in fatigue.

## 5.2. Murakami's model

Murakami's model [16] can be used to predict the fatigue strength using the defect size and the hardness value:

$$\sigma^D = \frac{A(H_v + 120)}{(\sqrt{\text{area}})^{1/6}} \quad (2)$$

with  $A = 1.43$  for surface defects. The projected area is defined in Eq.

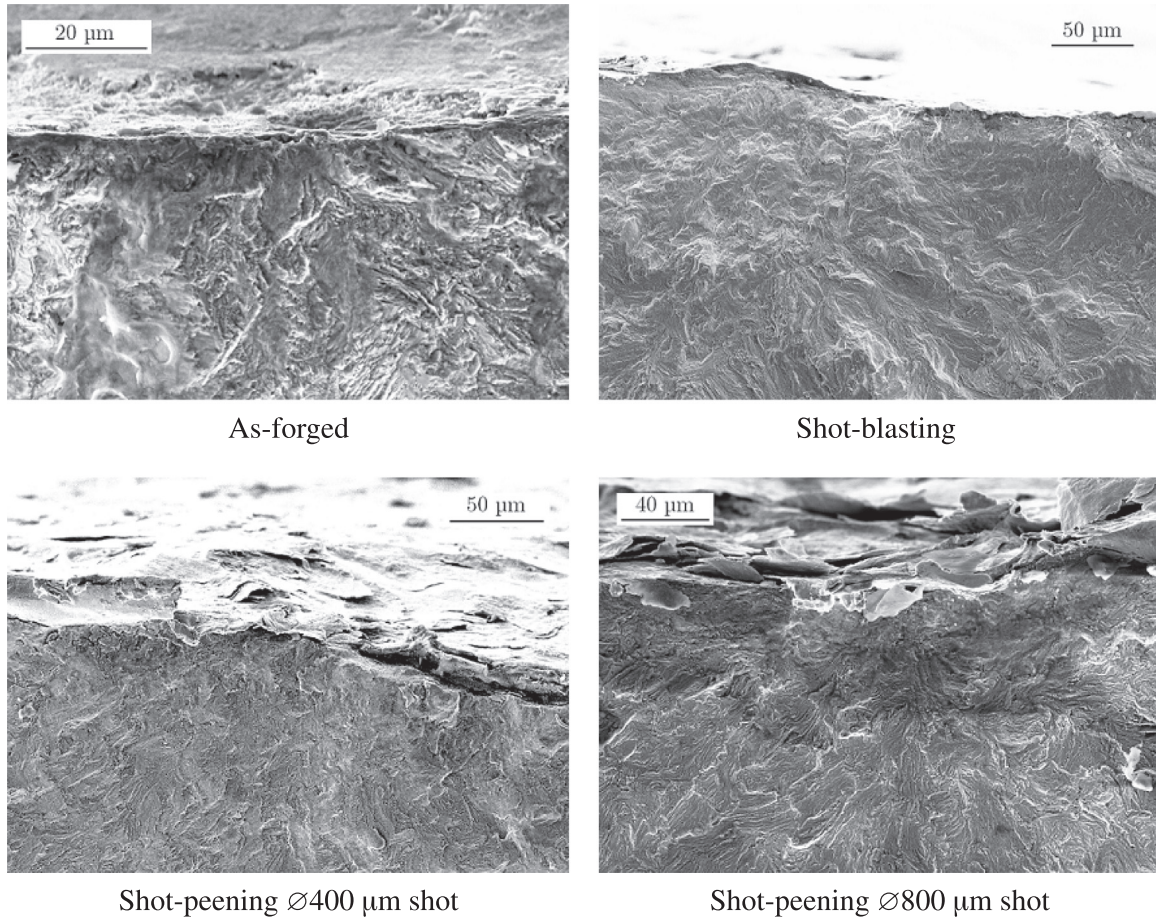


Fig. 13. SEM images of fracture surfaces showing the crack initiation location for each batch.

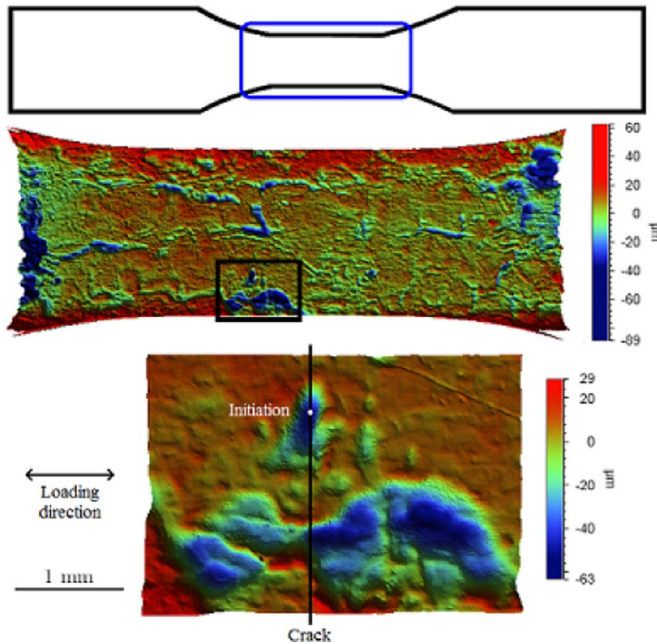


Fig. 14. Surface scan of the as-forged specimen from Fig. 12, showing a close-up of the critical defect. Crack initiation and crack path are indicated.

(1).

However, this model shows a very conservative prediction compared to the experimental values for the as-forged batch (Fig. 17). The model can be fitted to the as-forged values using  $A_{As-forged} = 1.91$ . This

fitted curve shows that the as-forged batch follows the 1/6 slope of the model. This model predicts a critical defect size of 41  $\mu\text{m}$ , which cannot be experimentally confirmed as no specimen had a crack initiation on a defect smaller than this value.

Using this model with the hardness value of the shot-blasted (or shot-peened) surface (350  $H_V$ ) shows that the increased hardness is not enough to correctly predict the shot-blasted and shot-peened fatigue strength values (Fig. 17).

These results show that taking into account the hardening introduced by the shot-blasting and shot-peening is not enough and that the residual stresses must be included in order to accurately model the fatigue strength values.

Murakami's model considers that the defects with the greatest projected area have the most influence in fatigue. However, the experimental results show that this is not always the case. Fig. 18 shows the surface scan of the critical defect of an as-forged specimen. Next to the critical defect are two larger defects which did not initiate a crack. The projected area for each defect is given in Table 5. The values show that defect n°3 has a greater projected area, which means that according to Murakami's model, this defect should have been the critical defect. A different criterion is therefore needed in order to explain why defect n°1 is the critical defect. Peterson [18] suggested a way of determining the stress concentration factor of an elliptical notch:

$$K_t = 1 + 2 \sqrt{\frac{t}{\rho}} \quad (3)$$

where  $t$  is the depth of the notch and  $\rho$  is its curvature radius in the loading direction. Where the two models differ the most is that Murakami considers the defect size only in the direction perpendicular

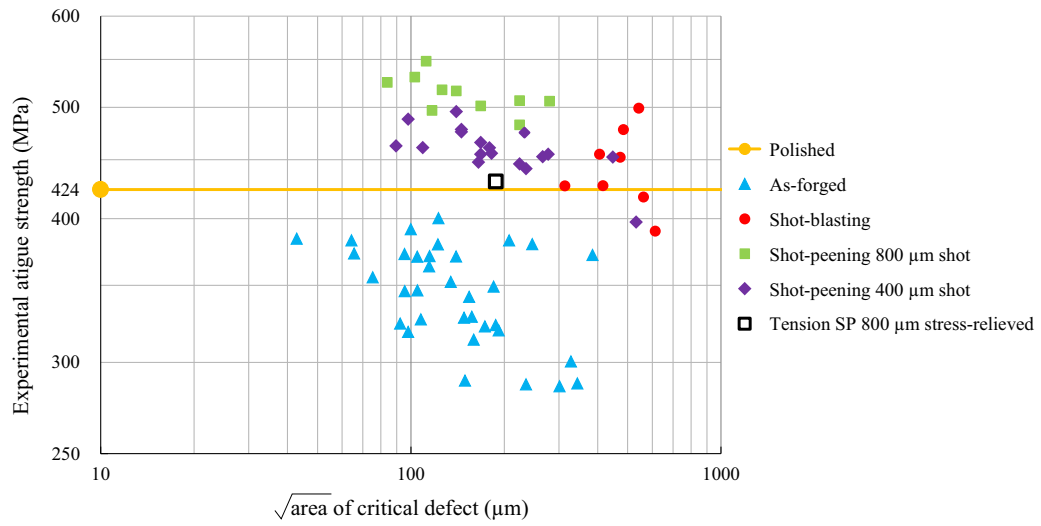


Fig. 15. Kitagawa diagram of the fatigue tests, with fatigue strength and critical defect size of each valid specimen.

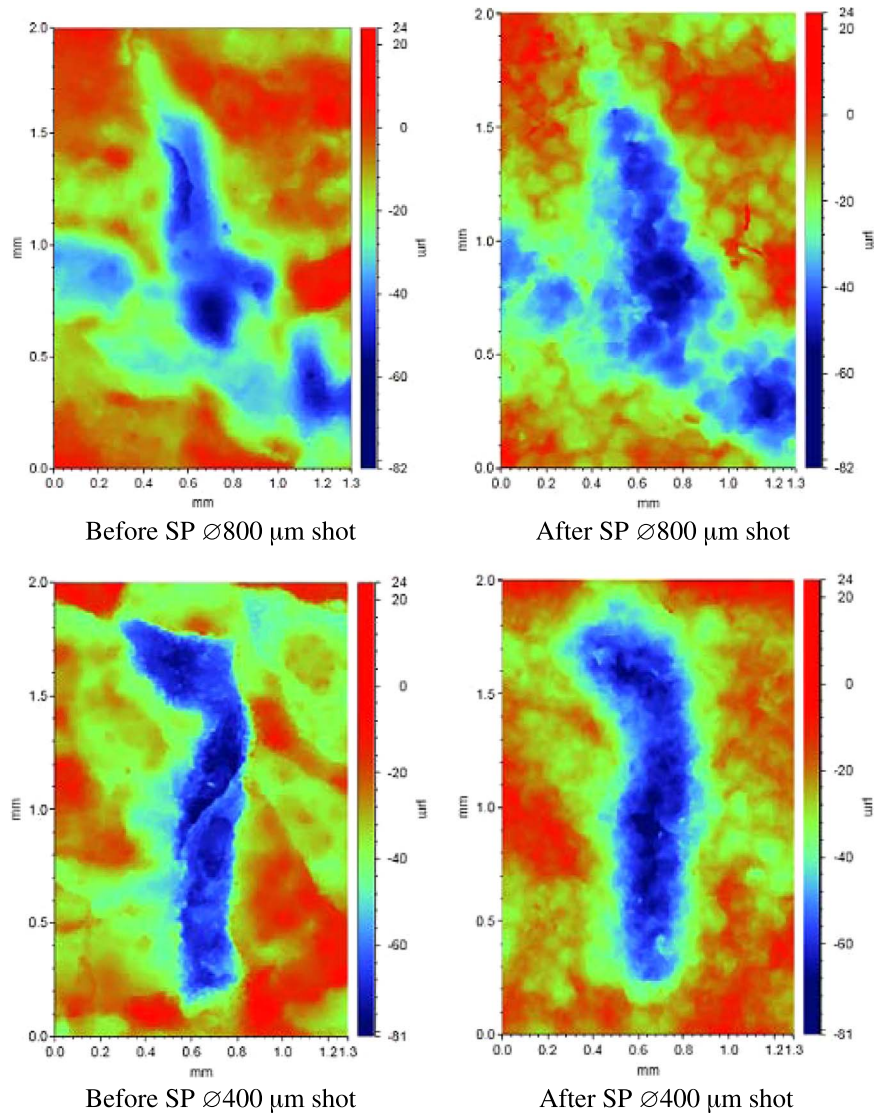


Fig. 16. Surface scans of a forging defect, before and after shot-peening.

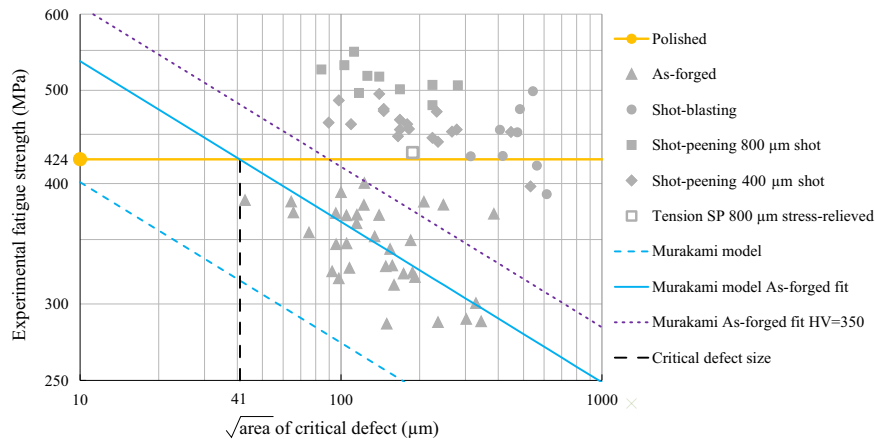


Fig. 17. Kitagawa diagram of the fatigue tests showing the Murakami model curves.

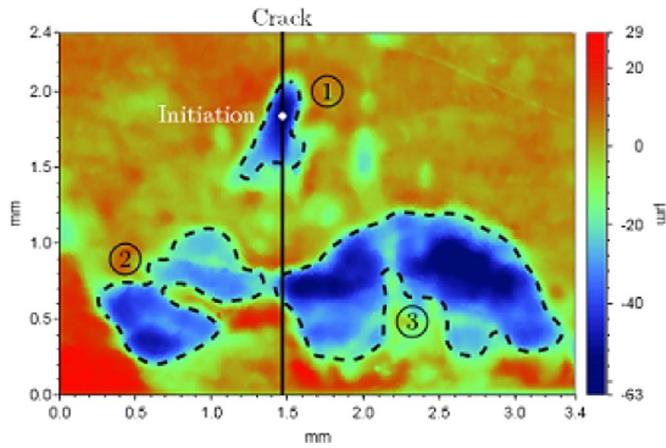


Fig. 18. Surface scan of the critical defect of the specimen shown in Fig. 14. The three major defects are outlined and numbered.

Table 5

Projected area and  $K_t$  for the three defects shown in Fig. 18.

Defect number	$\sqrt{\text{area}}$ (m)	$K_t$ Peterson
1 (critical defect)	153.0	2.01
2	85.5	1.61
3	176.6	1.47

to the loading direction, while Peterson uses the geometrical properties along the loading direction. The  $K_t$  values for the three defects (Table 5) show that the critical defect has the highest  $K_t$ . The influence of a defect is therefore determined not just by its size, but also by its sharpness in the loading direction. Further work must be done in order to determine the defect's geometric parameters which are the most influential on fatigue behaviour.

## 6. Conclusion

This experimental study was performed on specimens machined out of industrial components. The first part of the study was the thorough characterisation of the surface integrity of the specimens. The as-forged surface shows complex networks of defects which appear during forging.

Shot-blasting and shot-peening heavily alter the surface integrity, generating a microstructure gradient. Surface hardness is increased by around 60  $H_V$  and highly compressive residual stresses are also introduced ( $-500$  MPa on the surface). The forging defects are not erased but the shot impacts change the surface topography.

Fatigue tests were then performed to quantify the effect of the surface integrity on fatigue behaviour. The fatigue results show that the surface integrity has a major impact on fatigue behaviour: large forging defects and shot-blasting both affect fatigue strength. The forging defects are detrimental in fatigue and lower the fatigue strength with larger defects having a greater impact. The fatigue results show a large dispersion because of the varied surface defects.

Shot-blasting is used to clean the specimens of the forging scale, but has a large beneficial impact on the fatigue strength. A large part of this effect is due to the residual stresses introduced during shot-blasting (and shot-peening).

The fatigue strength of the shot-peened specimens is quite close to that of the shot-blasted specimens. This shows that for the shot-peening parameters chosen for this study, shot-peening and shot-blasting have an equivalent effect on fatigue behaviour.

The experimental tests are the first part of a larger study: the results will be used in subsequent studies to develop a fatigue model taking into account the effect of both the defects and shot-peening.

## Acknowledgements

This work has been performed within the ANR (National Research Agency) DEFISURF project, in a partnership including several industrial (Ascometal, CETIM, Renault, Transvalor, Atelier des Janves, Gévelot Extrusion) and academic (INSA Lyon MATEIS, ENSMP-CEMEF, Arts et Métiers ParisTech LAMPA) institutions.

## References

- [1] K. Lange, ed. Handbook of metal forming, Dearborn, Michigan: Society of Manufacturing Engineers, 1985.
- [2] E. Pessard, B. Abrivard, F. Morel, F. Abroug, P. Delhaye, The effect of quenching and defects size on the hcf behaviour of boron steel, *Int. J. Fatigue* 68 (0) (2014) 80–89.
- [3] M.J. Gildersleeve, Relationship between decarburisation and fatigue strength of through hardened and carburising steels, *Mater. Sci. Technol.* 7 (4) (1991) 307–310.
- [4] M.F. Garwood, M. Gensamer, H.H. Zurburg, J.T. Burwell, M.A. Erickson, F.L. La Que, Interpretation of Tests and Correlation With Service, American Society for Metals, 1951.
- [5] S.A. McKelvey, A. Fatemi, Surface finish effect on fatigue behavior of forged steel, *Int. J. Fatigue* 36 (1) (2012) 130–145.
- [6] A. Gariépy, F. Bridier, M. Hoseini, P. Bocher, C. Perron, M. Lévesque, Experimental and numerical investigation of material heterogeneity in shot peened aluminium alloy AA2024-T351, *Surf. Coat. Technol.* 219 (0) (2013) 15–30.
- [7] M.S. Bhuiyan, Y. Mutoh, A.J. McEvily, The influence of mechanical surface treatments on fatigue behavior of extruded az61 magnesium alloy, *Mater. Sci. Eng.: A* 549 (0) (2012) 69–75.
- [8] J. Sakamoto, Y.-S. Lee, S.-K. Cheong, Effect of fibprocessed sharp flaw on fatigue limit of shot peened medium carbon steel, In: L. Wagner (Ed.), Proceedings of the 12th International Conference on Shot Peening, Institute of Materials Science and Engineering, 2014, (pp. 8689).
- [9] J. Sakamoto, Y.-S. Lee, S.-K. Cheong, Effect of surface flaw on fatigue strength of

shot-peened medium-carbon steel, *Eng. Fract. Mech.* 133 (2015) 99–111.

- [10] R. Fathallah, A. Laamouri, H. Sidhom, C. Braham, High cycle fatigue behavior prediction of shot-peened parts, *Int. J. Fatigue* 26 (10) (2004) 1053–1067.
- [11] Y. Feng, S. Hu, D. Wang, L. Cui, Formation of short crack and its effect on fatigue properties of ultrasonic peening treatment S355 steel, *Mater. Des.* 89 (2016) 507–515.
- [12] W.J. Dixon, A.M. Mood, A method for obtaining and analyzing sensitivity data, *J. Am. Stat. Assoc.* 43 (1948) 109–126.
- [13] B. Gerin, E. Pessard, F. Morel, C. Verdu, A. Mary, Beneficial effect of prestrain due to cold extrusion on the multiaxial fatigue strength of a 27MnCr5 steel, *Int. J. Fatigue* 92 (2016) 345–359.
- [14] E. Pessard, F. Morel, D. Bellett, A. Morel, A new approach to model the fatigue anisotropy due to non-metallic inclusions in forged steels, *Int. J. Fatigue* 41 (2012) 168–178.
- [15] M. Kang, Y. Aono, H. Noguchi, Effect of prestrain on and prediction of fatigue limit in carbon steel, *Int. J. Fat.*, 29(911), 1855–1862. *Fatigue Damage of Structural Materials VI in: Proceedings of the Sixth International Conference on Fatigue Damage of Structural Materials*, 2007.
- [16] Y. Murakami, M. Endo, Effects of hardness and crack geometries on  $\Delta K_{th}$  of small cracks emanating from small defects, in: K. Miller, E. De Los Rios (Eds.), *The Behaviour of Short Fatigue Cracks*, London, MEP Publications, 1986, pp. 275–293.
- [17] H. Kitagawa, S. Takahashi, Applicability of fracture mechanics to very small cracks or cracks in the early stage, in: *Proceedings of the second international conference on the mechanical behaviour of materials*. ASM, 1976, pp. 627–631.
- [18] R.E. Peterson, *Stress Concentration Factors*, John Wiley and Sons, New York, 1974.